Langmuir monolayers of C_{17}, C_{19}, and C_{21} fatty acids: Textures, phase transitions, and localized oscillations

Salvador Ramos and Rolando Castillo[a)]
Instituto de Fisica, UNAM, P.O. Box 20-364, D.F. 01000, Mexico

(Received 19 October 1998; accepted 14 January 1999)

The phase diagrams of Langmuir monolayers of heptadecanoic (C_{17}), nonadecanoic (C_{19}), and heneicosanoic (C_{21}) acids have been determined from pressure-area isotherms, and from direct observations of the monolayers using Brewster angle microscopy. In this paper, we describe the observed domains, textures and phase boundaries for all mesophases presented by these fatty acids between 2° and 45 °C. The phase diagrams of the three fatty acids can be superposed moving the temperature scale according to the number of carbons in the tail of the fatty acids. The L_2/Ov phase transition, which is not detected through isotherms, was observed in all the fatty acids under study. At low temperatures, CS,L_2', and L_2'' phases of C_{21} were observed, as well as, the transitions among them. Also, we observed in C_{21} a new phase located among the phases L_2,L_2', and L_2''. This phase was found recently, in the relative same place, in the fatty acid C_{20} with a tilting azimuth between the nearest-neighbor and the next nearest-neighbor directions. In the crystalline phases of the monolayer of C_{21}, L_2'' and CS, we observed localized oscillations. These localized oscillations can be observed by long periods of time. The number of localized oscillations in the monolayer can be modified by long periods of relaxation or by heat treatment. Our results seem to indicate that these localized oscillations are areas with high density of defects, expelling material out of the monolayer. Therefore, they could be important in the events previous to the collapse. © *1999 American Institute of Physics.* [S0021-9606(99)71714-9]

I. INTRODUCTION

Phase diagrams of Langmuir monolayers of fatty acids on the surface of water have been studied intensively for decades. Nevertheless, significative advances have been obtained only in the last years due to new experimental techniques. X-ray diffraction (XRD), using intense and highly collimated x-rays available from synchrotron, gives the most explicit information about the monolayer organization.[1] Nevertheless, this kind of experiment is time consuming and expensive to obtain an entire phase diagram. Other powerful techniques have been developed to study monolayer organization, such as, polarized fluorescence microscopy (PFM)[2] and Brewster angle microscopy.[3,4] These techniques complement the information given by XRD experiments, since they survey larger scales ($>1\ \mu$m) providing information about homogeneity, textures, structure, and dynamics of monolayers. These optical techniques are quite sensible for observing very fine details in phase transformations such as molecular tilting. All these new experimental techniques have revealed that singularities in the surface pressure-area isotherms, observed since the time of Stenhagen[5] and Lundquist,[6,7] are due to phase changes. Each phase has a different molecular organization. Bibo, Knobler, and Peterson[8] have shown that molecular organization of condensed phases in fatty acid monolayers can be seen as a direct analog of some specific smectic phases. Thus, each phase can be described in term of four order parameters. These parameters are:[11,12] (a) positional order; (b) bond or lattice orientational order; (c) tilt order, which is the order of the molecular tilt azimuth with respect to the local orientational order; (d) herringbone order or broken axial symmetry, which is the staggered ordering of the planes of all-trans hydrocarbon chains. For these order parameters a distinction has been made between quasi-long-range order, in which the order decays accordingly to a power law, and short-range order where the order falls off exponentially with distance.

Among the experimental techniques mentioned above, Brewster angle microscopy[3,4] probably is the best suited to be used in direct observations during compression of monolayers, in a Langmuir trough. This is a technique based on the study of the reflected light coming from an interface illuminated at the Brewster angle, by a laser beam polarized in the plane of incidence *(p)*. When the angle of incidence of the laser beam is the Brewster angle, there is no light reflected, from a clean and perfect interface, i.e., the refractive index changes abruptly form one medium to another. For a real interface which has a transition region where the refractive index changes smoothly form one value to another, the reflected intensity at the Brewster angle is a minimum, but it does not vanish completely. The reflected intensity depends strongly on the interfacial characteristics, such as, molecular density and molecular anisotropy. These properties are particularly modified when a monolayer is located at the interface. Thus, a monolayer on an interface is able to produce reflection of light. In tilted phases, the anisotropy is sufficiently strong to have enough light reflection to make quite visible the mosaic of textures due to tilted domains. In un-

[a)]Electronic mail: rolandoc@fenix.ifisicacu.unam.mx

tilted phases with rectangular lattice symmetry, textures are also visible, but with much less contrast. This is probably due to the anisotropy of the unit cell (herringbone alignment). Phase transitions are visible either as a dramatic change in the degree of contrast or as a sudden alteration of the mosaic of textures and domain borders. Many of the textures and domain morphologies found in monolayers using the Brewster angle microscope (BAM), have been explained using model calculations of monolayers with tilted molecules.[9,10,26]

The work of many different groups has contributed to obtain a general picture of the phase diagram of fatty acid monolayers, as well as, the structure of their phases using XRD, PFM, and Brewster angle microscopy. This picture can be reviewed as follows: At very low surface densities, when the average area per molecule, a, is much larger than the cross section area of an isolated molecule, an amphiphilic monolayer behaves as a two dimensional gas. Here, a molecule in a monolayer is still free to show all the conformational entropic contribution without any interference from neighbors. A first-order phase transition from the gas phase to a liquid-expanded (LE) phase is observed upon compression of the monolayer. LE phase is isotropic and molecules are tilted. The gas-phase side of the transition is of the order of $a=300-1500$ Å^2/molec, whereas on the LE side a is of the order of the cross section area of an isolated chain ($30-40$ Å^2/molec). A second phase transition to a liquid condensed (LC) state is observed upon further compression of the monolayer; a is of the order of $22-25$ Å^2/molec. Here, a is just barely larger than the cross sectional area of a fully stretched (all-trans) chain. Actually, condensed phase is made up of a variety of mesophases, i.e., phases where the translational order of the molecules is short ranged and the orientational order of the bonds between the molecules is long range. At low surface pressures, there are several phases showing molecular tilt with distinct symmetry. L_2 phase has a collective tilt towards a nearest neighbor (NN).[14,16,20–22,24,30] $L_2^{'}$ and Ov phases tilt to a next-nearest neighbor (NNN) molecule.[14,16,20,22,24,30] The L_2/Ov transition is quite peculiar, since it was found through BAM observations only,[17] since it cannot be detected with surface pressure-area isotherms, due to the lack of an area/molecule change during the transition.[16] At high pressure, there are two untilted phases, the super liquid phase, LS,[19–21,25] and the solid phase, S.[14,19,20,23] Structure of mesophases can be locally hexagonal (LS) or distorted hexagonal, i.e., centered rectangular (L_2, $L_2^{'}$, Ov, S). In addition to mesophases, crystalline phases have been found with a positional quasi-long-range order. They show positional correlations larger than 500 Å. They are CS and $L_2^{''}$ phases, both are centered rectangular with herringbone order. $L_2^{''}$ is at two-dimensional crystal with a NN-tilt[14] and CS is untilted.[14,22–25] At very high pressures, all phases collapse in multilayers. The details of the multilayering process are quite unknown. Textures of condensed phases and the precise coexistence lines between phases have been obtained mainly using PFM and Brewster angle microscopy. This is the case for $L_2/L_2^{'}$ and $L_2^{''}/CS$ transitions,[15] for $L_2/L_2^{'}/L_2^{''}$ transitions,[27] and many more presented with detail by Rivière *et al.*[18]

Tilt to an intermediate direction breaks the chiral symmetry of a monolayer. The breaking of inversion symmetry allows nonchiral molecules to arrange in chiral structures. Phases in which molecular tilt is intermediate between NN and NNN directions have been observed. Durbin *et al.*,[13] have found a intermediate phase (I) for a monolayer of eicosanoic acid (C_{20}) using surface pressure-area isotherms and x-ray diffraction. These authors also found that the transition from I phase to an NN-tilted structure is first order, with a $\sim 60°$ change in the tilt direction, whereas, the transition to an NNN-tilted structure is apparently continuous.

In this paper, we will present a detailed study to obtain all the boundaries in the phase diagrams of three fatty acids: Heneicosanoic (C_{21}), nonadecanoic (C_{19}), heptadecanoic (C_{17}), in the temperature range of $2-45\,°C$. A partial phase diagram of C_{21} has been presented by Fischer *et al.*[29] Also for C_{21}, Teer *et al.*[28] have presented a whole phase diagram, which has been obtained by shifting the temperature axis ($6\,°C$ per methylene group) from other phase diagrams previously reported.[18] Our phase diagrams were determined using surface pressure-area isotherms and BAM observations. Therefore, in this paper, we will show the mosaic of texture of the phases as observed with the BAM, as well as, the phase transitions between those phases. Fatty acids with an odd carbon tail have been less studied than the case of even carbon tail acids. For the case of C_{17}, we present the change of textures during the phase transformations: L_2-Ov, $Ov-LS$, and L_2-LS. As far as we know, they are not previously reported. The same phase changes are presented for C_{19}, although we included the $L_2-L_2^{'}$, $L_2^{'}-LS$, and $L_2^{'}-S$ transitions. C_{21} is the richest phase diagram, since in addition to the mentioned phase transitions, we observed the $L_2-L_2^{''}$ and the $L_2^{''}-CS$ transformations at low temperatures. Also, we will report here a new intermediate phase for C_{21}, which has been reported quite recently for the case of C_{20}.[13] In addition, we will present an outstanding observation made with the BAM in C_{21}, which has not been reported before, as far as we know. We observed localized oscillations in the monolayer, in the crystalline phases $L_2^{''}$ and CS. Localized oscillations are related to energy and stress concentration in some relative large areas with high concentration of defects in the monolayer. They could be important in the events previous to the collapse.

II. EXPERIMENT

C_{17} (97%), C_{19} (99%), and C_{21} (99%) were purchased from Aldrich (U.S.A.), and they were used without any further purification. With the aid of an spreading solution, fatty acids were spread onto a subphase of ultrapure water (Nanopure-UV) at pH=2. The spreading solution was made with chloroform (Aldrich U.S.A., HPLC). HCl (Merck, Mexico) was used to modify pH.

All monolayers were prepared on a computerized Nima Langmuir–Blodgett trough (TKB 2410A, Nima Technology Ltd., England) using a Wilhelmy plate to measure the surface pressure $\Pi=\gamma_0-\gamma$, i.e., the surface tension difference of the

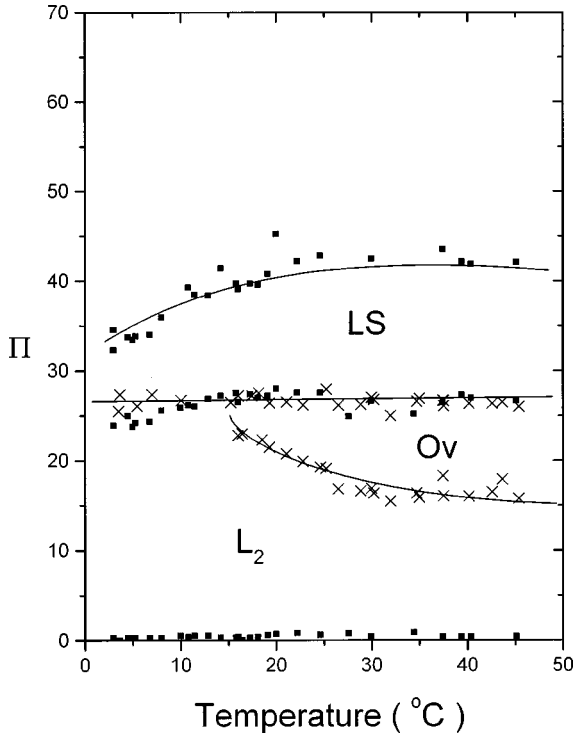

FIG. 1. Surface pressure-temperature phase diagram for C_{17} fatty acid monolayer. The phase changes were obtained from our $\Pi - a$ isotherms (■) and BAM observations (×).

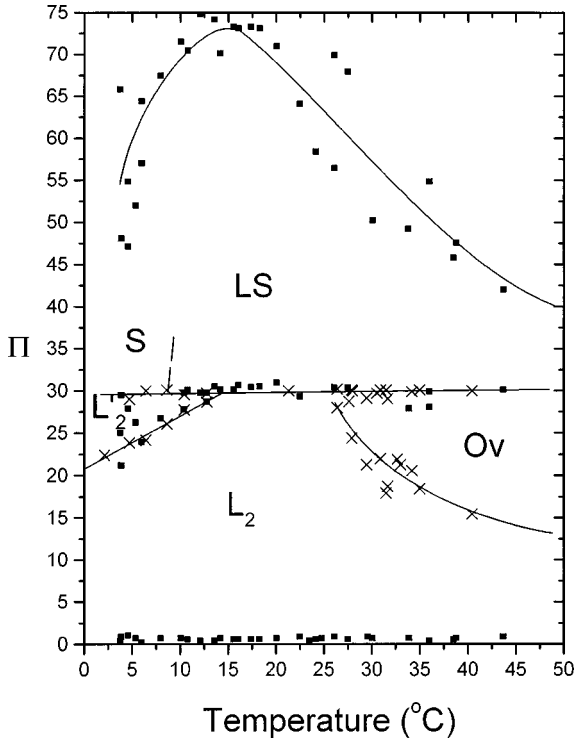

FIG. 2. Surface pressure-temperature phase diagram for C_{19} fatty acid monolayer. The phase changes were obtained from our $\Pi - a$ isotherms (■) and BAM observations (×).

clean subphase and that of the amphiphile covered subphase. The trough is isolated from vibrations using a pneumatic tube incorporated into a steel base. The barriers are made of polytetrafluoroethylene (PTFE) fitted with stiffening bars defining a working circular area starting at 1000 cm^2. All experiments were carried out in a dust-free environment. The speed of compression was in the range of 1–5 $Å^2$/molec.min.

The BAM observations were performed using a BAM1 (Nanofilm Technologie GmbH, Germany) with a spatial resolution of ~ 4 μm. The BAM analyzer gave the best contrast while kept at $\sim 0°$ or $\sim 180°$.

The Nima LB trough and the BAM were placed on a concrete table cemented to the ground floor of our building. Temperature in the trough was kept constant with the aid of a water circulator bath (Cole-Parmer 1268-24, U.S.A.).

III. RESULTS AND DISCUSSION

A. General features

Figures 1–3 show the different phases found for C_{17}, C_{19}, and C_{21}, in the range of temperatures worked in this study (2–45 °C). The coexistence lines were obtained from the temperatures and the pressures, where phase changes do occur. The phase changes were determined from our $\Pi - a$ isotherms and from BAM observations. The three phase diagrams are displaced in some regular fashion. They follow the known rule that the addition of one CH_2 group to the tail of a fatty acid, displaces the phase boundaries to higher temperatures by a value in the range of 5–8 °C.

We identified the phases for the three fatty acids studied here, with the aid of the information given for the even carbon tail acids mentioned in the Introduction. The C_{17} monolayer (Fig. 1) presents three phases in the worked temperature range: L_2, LS, and the relative new Ov phase. For surface pressures above 35–45 mN/m the monolayer is collapsed. The C_{19} monolayer (Fig. 2) presents five phases in the worked temperature range: L_2', L_2, Ov, S, and LS. The monolayer collapses for surface pressures above 45 mN/m, at low temperatures. The collapse occurs at pressures of the order of 70 mN/m for temperatures in the range of $10-25\,°C$. At higher temperature, the collapse pressure falls down as temperature is increased. As expected, the C_{21} monolayer (Fig. 3) presents the richest phase diagram, because high-density phases can be observed. The phases presented in Fig. 3 are: L_2'', L_2', L_2, Ov, CS, S, and LS. Here, we also included the $\Pi - a$ isotherm data of Lin *et al.*[14] In this phase diagram, we also show a phase I, where the boundary with L_2 was obtained with isotherms and the boundary with the L_2' was determined with BAM observations. In the same relative place of the phase diagram, recently, Durbin *et al.*[13] have reported a similar phase for C_{20} fatty acid using XRD. The molecular tilt of this new phase is intermediate between NN and NNN directions. They named this phase as I phase, so we did the same for C_{21}. The C_{21} monolayer presents the collapse when Π reaches values of the order of 60 mN/m.

In BAM images, all tilted phases L_2, Ov, L_2', and L_2'' show the same general pattern: A mosaic of irregularly shaped domains. The contrast between domains comes from the different tilting of the all-trans hydrocarbon tails. This contrast is relatively strong in tilted phases. Each shade of

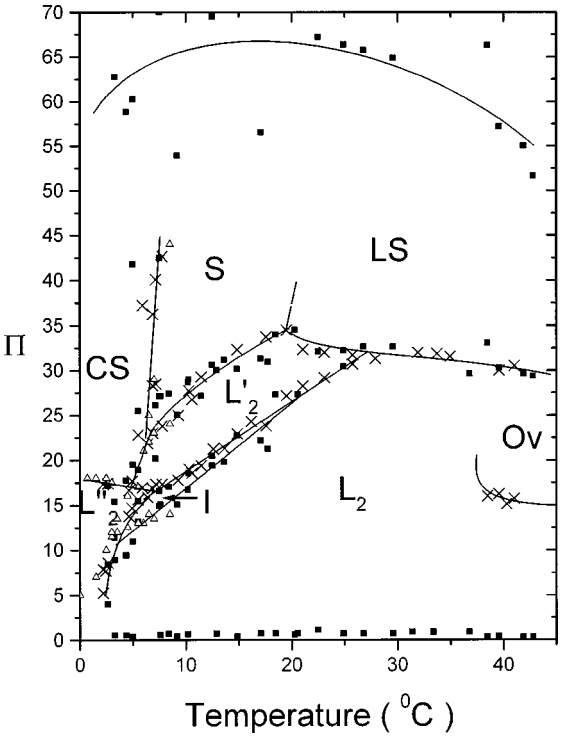

FIG. 3. Surface pressure-temperature phase diagram for C_{21} fatty acid monolayer. The phase changes were obtained from our $\Pi - a$ isotherms (■) and BAM observations (×). Here, we included the $\Pi - a$ isotherms data from Lin *et al.*[14] (△).

gray corresponds to a different azimuthal tilt direction. At low pressure, in L_2, the contrast is quite large and the mosaic pattern is outstanding. As temperature is lowered the contrast decreases. Also, at low temperatures, the number of mountain-shaped structures and Newton rings increase. These structures are multilayers defects, since it is not possible to focus them, and they do not change rotating the polarizer. The number and occurrence of these mountain-shaped structures or Newton rings depend on how the monolayer is compressed. We will come back to this issue in more detail below. The untilted phases *S* and *CS* also present a mosaic of textures, but with a very low contrast between their domains. Here, each shade of gray corresponds to a different lattice orientation of the all-trans alkane chains (herringbone order). *LS* is a phase where the contrast is completely lost in BAM images. This is consistent with the untilted hexagonal lattice symmetry of this phase. Here, the molecules could be rotating freely (rotator structure).[19,20]

B. Phase transitions

We have followed here, the method for grouping monolayer phase transitions used by Rivière *et al.*[18] Therefore, our phase transition observations were grouped into four categories described below. Some phase transitions will be illustrated with BAM images. In all the images, we have a few multilayer defects in the field of view (like Newton rings or mountain-shaped structures), which do not disappear during the phase transition under discussion. These defects help us to assure that we are making observations in the same area of the monolayer, before and after the phase transition.

1. Transitions between an anisotropic and an isotropic phase ($L_2'-LS$, L_2-LS, $Ov-LS$, and $S-LS$)

L_2-LS and $Ov-LS$ transitions are visible as a lost of contrast when they are observed with the BAM, due to the lack of tilting in the hexatic *LS* phase. This lost of contrast corresponds to a big kink in the isotherm. These transitions are reversible and the mosaic pattern of the tilted phases are recovered on decompressing the monolayer, despite the domain boundaries in the *LS* phase have disappeared. The lost of contrast is gradual, but rapid in both transitions. This is consistent with a continuous decrease in the anisotropy of the monolayer. Figure 4 shows a compression–expansion cycle along the transition $Ov-LS$, for C_{17}. The defects shown in Fig. 4 for this monolayer do not change during the transition. Thus, in the field of view confined by those defects, we can easily see domains of the Ov phase with different shades of gray, at a pressure slightly below the transition pressure. These domains disappear when the transition $Ov-LS$ is reached and they reappear when the pressure drops again.

In C_{17} or C_{21}, it is not so easy to see domains growing in the L_2-LS phase transition, as in the case of C_{19}. In C_{19}, it is easy to see the how domains of the new phases (L_2 or Ov) grow when the monolayer is relaxing from above the coexistence line. i.e., when pressure drops and the monolayer reaches the coexistence line slowly. Figure 5 shows the lost of domains form L_2 phase when the pressure is increased and the L_2-LS transition is reached.

We classify L_2-LS and $Ov-LS$ transitions as first order. Because, when the monolayer is relaxing from slightly above the transition line, it is possible to see domains of the new tilted phases growing steadily. Also, there is hysteresis in the pressure of the phase change.

In C_{21} and C_{19}, the $L_2'-LS$ phase transition is seen in the BAM as a sudden loss of contrast. This transition also corresponds to a big kink in the isotherm. The images are quite similar to the case of L_2-LS or $Ov-LS$, therefore, a specific observation of this transition is not presented. It is usual to observe in the $L_2'-LS$ phase transition, the shortening of the L_2' domains during the compression. Nevertheless, the growing of domains is more clearly seen when the monolayer is relaxing from the *LS* phase. We classify this transition as first-order transition.

2. Transitions between a highly anisotropic tilted phase and a weakly anisotropic untilted phase ($L_2''-CS$, $L_2'-CS$, and $L_2'-S$)

In these phase transitions, the decrease in the level of contrast among domains is a common feature. However, the weak anisotropy in *S* and *CS* phases is visible to the BAM yet. In C_{21}, the $L_2'-CS$ transition can be seen in the BAM as a rapid growing of irregular domains many of them elongated and some with a needle shape [see Figs. 6(a) and 6(b)]. Isotherms show this transition with a big kink. Relaxing the monolayer from the *CS* phase allows us to see how the needle-shaped structures start to grow up to irregular domains, when the border of the L_2' is reached. These needle-

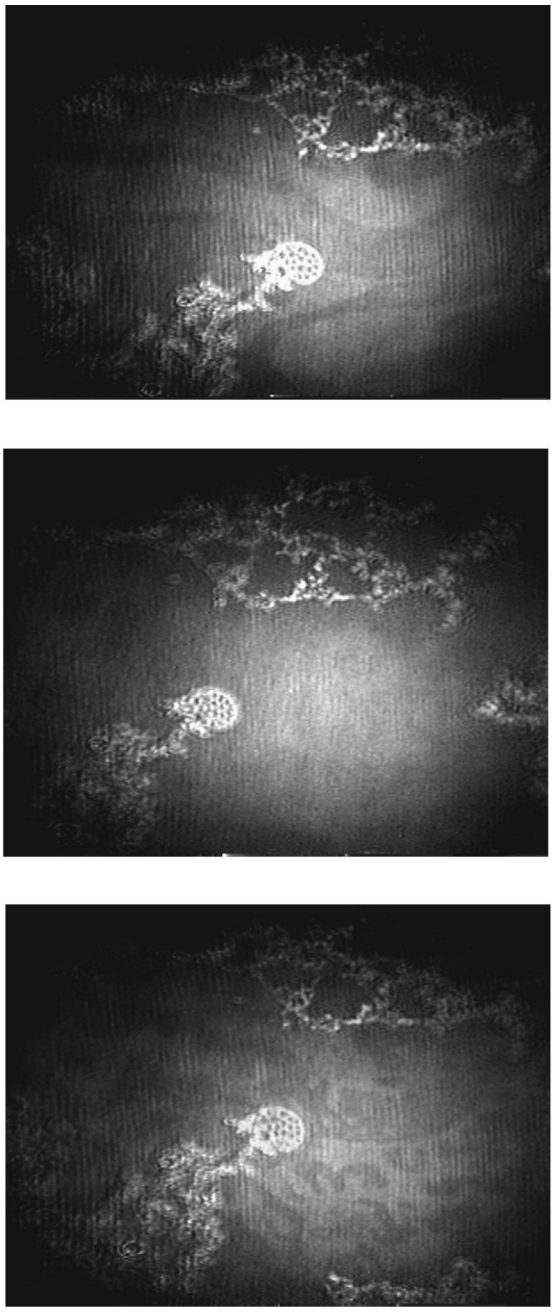

FIG. 4. Phases observed with the BAM in a compression-expansion cycle starting below the $Ov-LS$ phase transition ($T=16.0\,^{\circ}\mathrm{C}$ and $\Pi=27.1-27.3$ mN/m). Ov phase, upper panel ; LS phase, medium panel; Ov phase, lower panel.

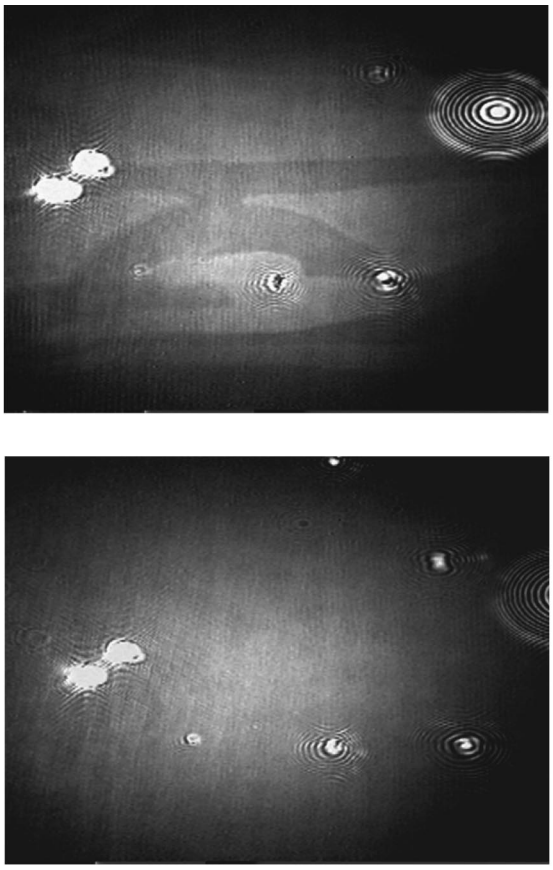

FIG. 5. Phases observed with the BAM in a compression starting slightly below the L_2-LS phase transition ($T=15.2\,^{\circ}\mathrm{C}$ and $\Pi=29.9$ mN/m). L_2 phase, upper panel; LS phase, lower panel.

shaped structures also appear in the transition $L_2''-CS$ [see Fig. 6(c)]. We classified both transitions as first order.

The $L_2'-S$ transition can be seen as a big kink in the isotherm and as a change in level of contrast in the BAM. This change is not as rapid as in the L_2-LS transition. Nevertheless, contrast is not lost completely as in the LS case. It is possible to see a mosaic pattern with a very low difference in contrast among domains, as well as, how the contrast is advancing in the field of view along the transition. We classify this transition as first order. BAM observations made possible to estimate where the boundary between S and LS phases is, due to the difference in contrast between LS and S phases. This boundary is shown in Fig. 2 for C_{19} ($\sim 8.6\,^{\circ}\mathrm{C}$) and in Fig. 3 for C_{21} ($\sim 19.50\,^{\circ}\mathrm{C}$).

3. Transitions between two anisotropic phases with approximately the same degree of anisotropy (L_2-L_2'', $L_2'-L_2''$, L_2-L_2', L_2-Ov, and $S-CS$)

Transition from L_2 to Ov is very clear using the BAM, whereas, it cannot be noticed with isotherms. In spite of the change from NNN to NN tilting, as mentioned in the introduction, during the transition the surface area/molecule does not change. Figure 7 presents an example of this transition for a monolayer of C_{17}, which is compressed and decompressed on several occasions, around the transition line. The change of domain shapes is evident in these pictures. Most of the times, in this kind of compression–decompression cycles, domains reform almost to the same shapes, suggesting some kind of memory. Figures 7(a) and 7(c) show this feature. Also there, we can observe how the monolayer evolves from domains with boundaries with many sharp kinks (L_2) to domains with boundaries with an irregular shape (Ov). In C_{19}, the contrast change is not so clear as in the case of C_{17}, but we can see the same features. In C_{21}, the L_2 phase is more fluid than in the other fatty acids. Thus, it is more difficult to observe the L_2-Ov transition. In this case, it is easy to mistake a phase transition with a rotation of the whole monolayer in the field of view of the BAM. Domains

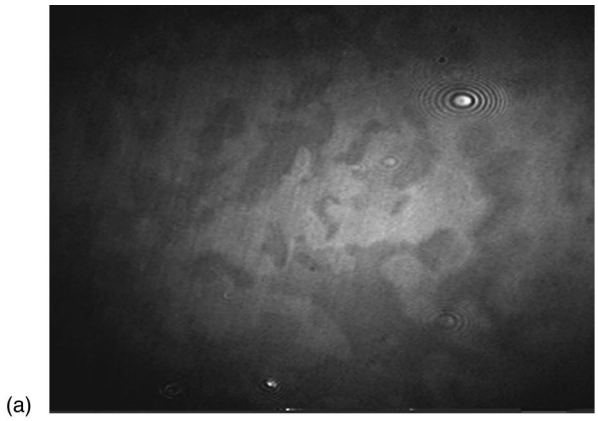

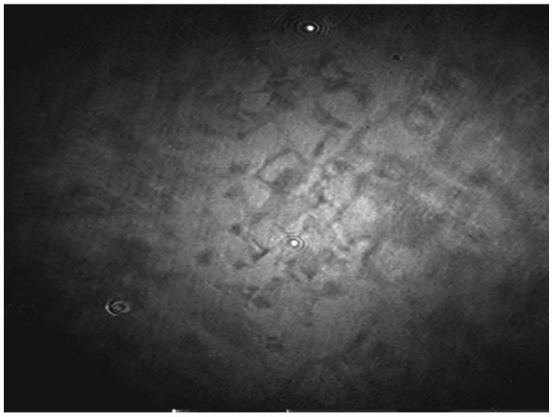

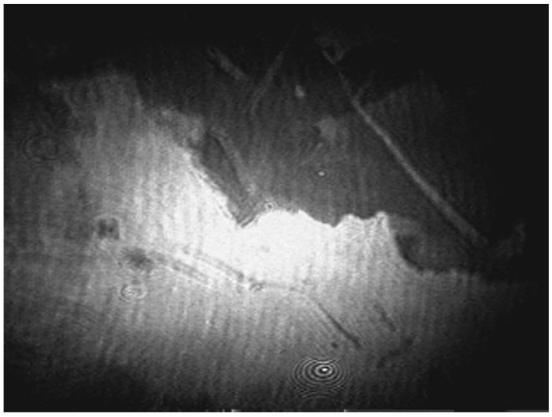

FIG. 6. Phases observed with the BAM close to the $L_2^{'}-CS$ and $L_2^{''}-CS$ phase transitions. $L_2^{'}$ phase as seen just below the transition, upper panel, and CS phase just above the transition, medium panel ($T=4.9\,^{\circ}\mathrm{C}$ and $\Pi=18.6$ mN/m). In the lower panel, we show $L_2^{''}$ phase just starting the transformation to CS phase ($T=2.2\,^{\circ}\mathrm{C}$ and $\Pi=19.0$ mN/m). Here, there is a light-gray needle-shaped structure, which suddenly appeared in the lower left part of the field of view, in the gray area.

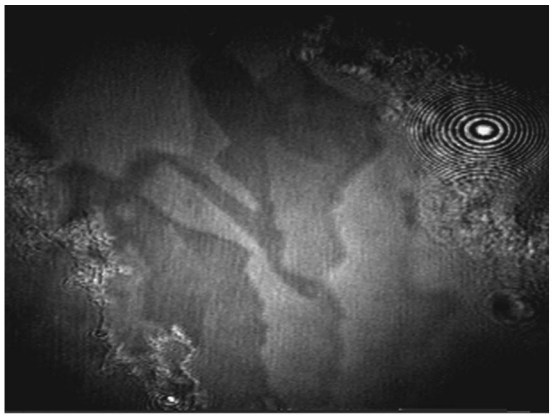

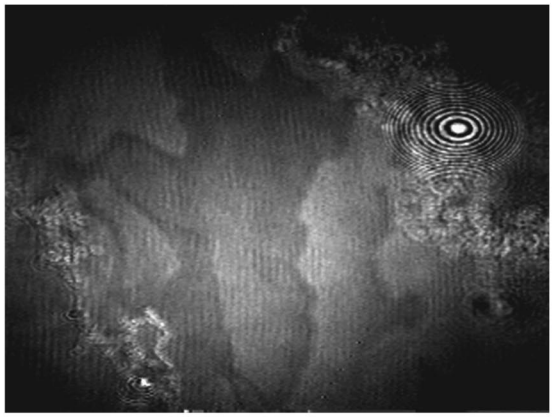

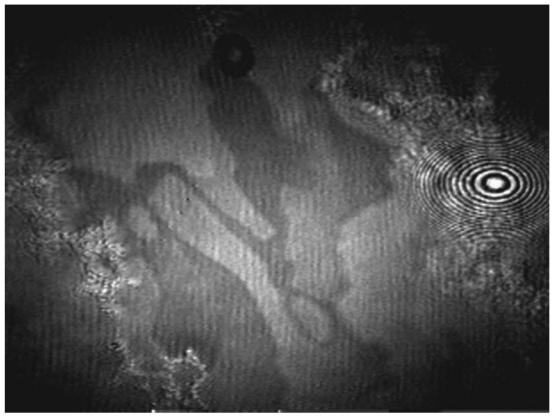

FIG. 7. Phases observed with the BAM close to the L_2-Ov phase transition at $T=22.8\,^{\circ}\mathrm{C}$ and $\Pi=19.4$–19.7 mN/m. (a) L_2 phase slightly below the phase transition; (b) When L_2 phase is compressed, the Ov phase appears; (c) Decompressing the monolayer, L_2 phase is recovered with almost the same domains.

can be seen disappearing steadily from one phase (L_2) to the other (Ov), decompressing the monolayer. All our observations are consistent with a first-order transition, in agreement with the observations of Rivière *et al.* In C_{21}, one part of the L_2-Ov boundary must be almost vertical since, it was impossible for us to catch more experimental points for this phase transition close to 37 °C. See Fig. 3.

The transition from $L_2-L_2^{'}$ was observed with the BAM in C_{19} and C_{21}. This transition is characterized by a change of domain shapes. The contrast between domains is low but clearly visible, as well as the phase transition. These features can be seen in Fig. 8. The low level of contrast is due to the same degree of anisotropy in both phases. We can see how rapid domains grow, decompressing the monolayer. We classify the transition as first order, however, the lack of contrast between domains does not allow to see the growing of domains as clearly as in other cases previously mentioned.

Compressing the L_2 phase of C_{21} fatty acid, at low temperature, allowed us to reach the outstanding phase transition

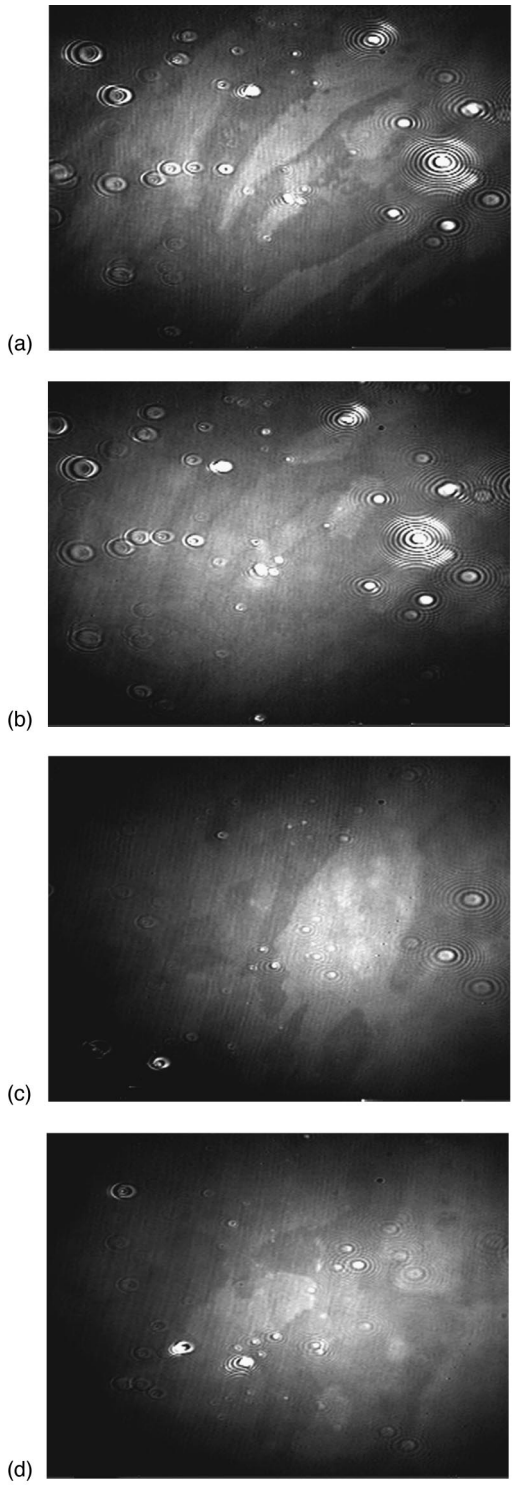

FIG. 8. Phases observed with the BAM close to the L_2-L_2' phase transition. C_{19} at $T=6.4\,^{\circ}\mathrm{C}$ and $\Pi=23.1$ mN/m: (a) L_2 phase and (b) L_2'. C_{21} at $T=21.0\,^{\circ}\mathrm{C}$ and $\Pi=26.5$ mN/m: (c) L_2 phase and (d) L_2'. In both cases, we can see the same place in the monolayer, if we use the defects as a guide to the eye. Defects do not changed during the phase transition.

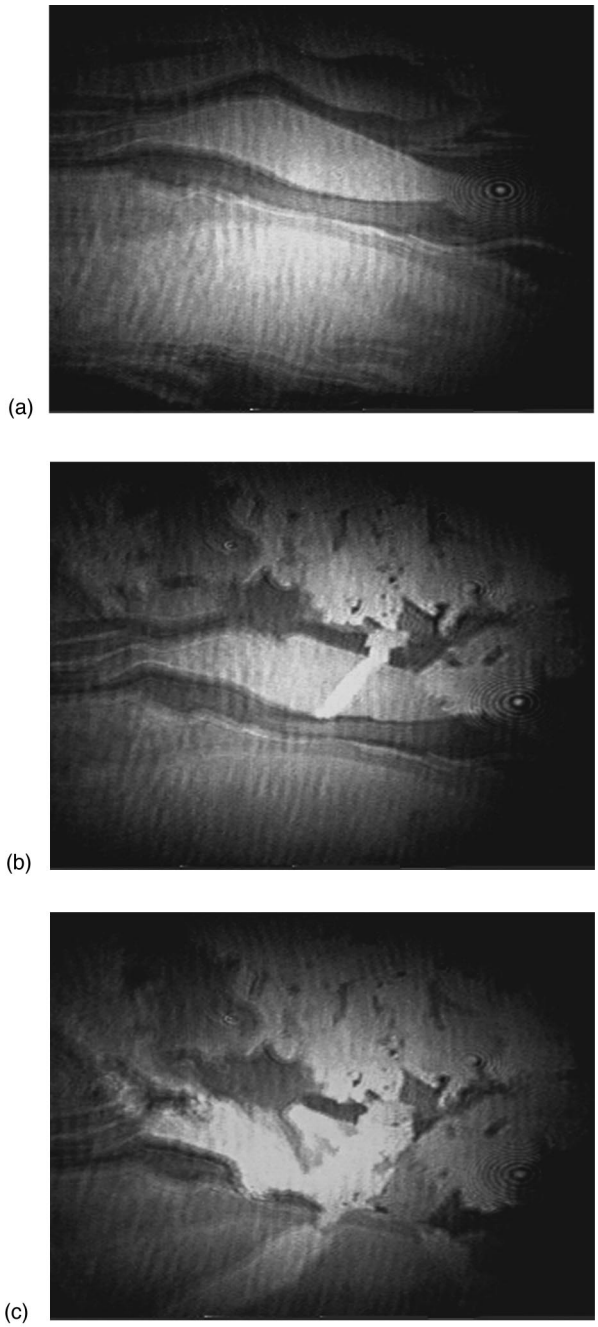

FIG. 9. Front passing along the field of view of the BAM in the L_2-L_2'' phase transition at $T=2.2\,^{\circ}\mathrm{C}$ and $\Pi=5.3$ mN/m. (a) L_2 phase before the transition; (b) the front, changing to the new L_2'' phase, is visible as bright irregular domains coming from above; (c) the front has reached the bottom of the field of view.

L_2-L_2''. Isotherms show this transition as a small kink. Here, suddenly, an irregular change of phase front passes along the field of view of the BAM. This front modifies the mosaic of domains. An observation of these events is presented in Fig. 9. The front travels quite rapid, but at a finite speed in the range of 150–550 μm/s. In some cases, previous to the pass of the front, a deformation of the domain pattern is observed. In other cases, it is possible to catch how the change of phase grows up from some regions, like a growing tree, propagating the change of phase front to rest of the field of view. Decompressing the monolayer, the domain pattern of L_2'' changes in a way which recalls a melting process. We classified this transition as a first-order transition.

In the $S-CS$ phase transition, a mosaic of irregular domains with a very low level of contrast among them, changes

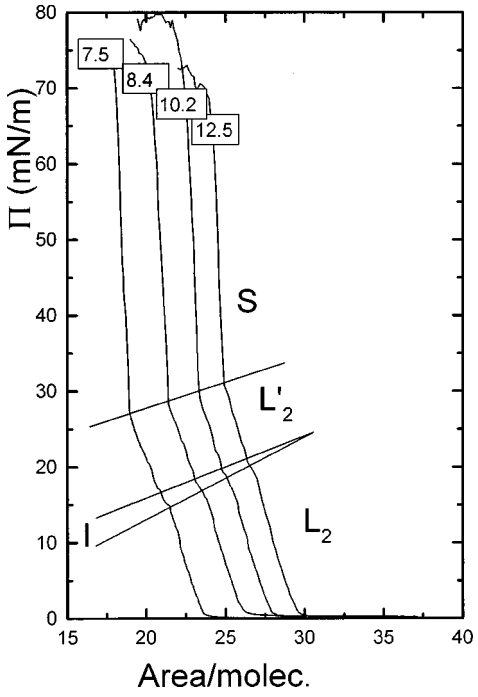

FIG. 10. Several $\Pi - a$ isotherms of the C_{21} fatty acid (temperatures are indicated in Centigrade scale). They show the main phase transformations for those temperatures, as well as the location of a new phase *I*. The area-axis labels are for the 7.5 °C isotherm; other isotherms are shifted horizontally proportionally to temperature for clarity.

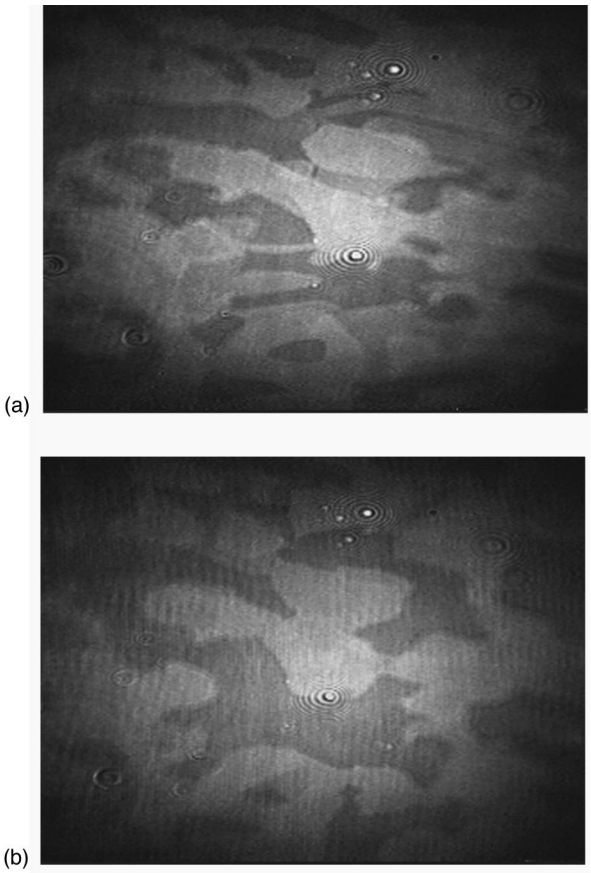

FIG. 11. Phase transition between $I-L_2'$ phases at $T=10.9\,°C$ and $\Pi = 19.2$ mN/m. Defects do not change along the transition, so they can be used as a guide to the eye to localize domain changes. (a) *I* phase slightly below the transition line, and (b) L_2' phase slightly above the transition line.

to another mosaic of domains, also with a very low level of contrast among domains. However, this transition is quite clear, and BAM images allow to see the needle-shaped domain characteristics of the *CS* phase. Isotherms show this transition with a small kink. In the $L_2''-L_2'$, we also observed a similar change from a mosaic of irregular domains to another mosaic of irregular domains. However, in this case the change occurs more rapid, and the level of contrast in L_2' is lower than in L_2''.

4. Transitions between tilted phases (NN or NNN) to some intermediate position

As mentioned above, all our observations suggest that there is a phase *I* in C_{21}, with an intermediate tilt between NN and NNN directions. One phase of this kind was observed in the same relative place in C_{20}, by Durbin *et al.*[13] In the present work, the phase transitions L_2-I and $I-L_2'$ were detected in several isotherms as small kinks. Nevertheless, they are not so clear to be a conclusive evidence. $\Pi - a$ isotherms showing these kinks are presented in Fig. 10. The transition between $I-L_2'$ can be observed easily with the BAM. An example is shown in Fig. 11. There is no big change in contrast along the field of view during this transition, although, there is a clear change in the mosaic of domains. In some cases, it is possible to observe how domains grow.

Our borderline for the L_2-I transition agrees with experimental points of Lin *et al.*[14] In the isotherms of those authors, there are some small rounded kinks slightly above their $C-D$ transition, in the temperature range of 7.0–8.5 °C. That could correspond to the $I-L_2$ phase transition. Nevertheless, this is not clear from their isotherms. They did not make any comment about this feature. Our observations with the BAM did not allowed us to give a clear-cut transformation line. This is rather a continuous transition, where some light gray domains darken slowly becoming dark gray domains. This goes into the direction of a second-order phase transition. Our observations about the order of the phase transitions do not agree with the work of Durbin *et al.*[13] They classify them in the reverse way, i.e., L_2-I as a first-order and $I-L_2'$ as a second-order phase transition.

C. Localized oscillations

In crystalline phases of the C_{21} monolayer, i.e., L_2'' and *CS*, it is possible to observe localized oscillations. These are localized holes surrounded by Newton rings, which are blinking, i.e., they appear and completely disappear suddenly in the same place of the monolayer. They can be observed along the monolayer at several parts of the field of view of BAM. In Fig. 12, we present an example of these localized oscillations in four different images, coming from the same area of observation in the monolayer. This images were obtained from our VCR tape observation records, where the elapsed time from the first image to the last one is less than

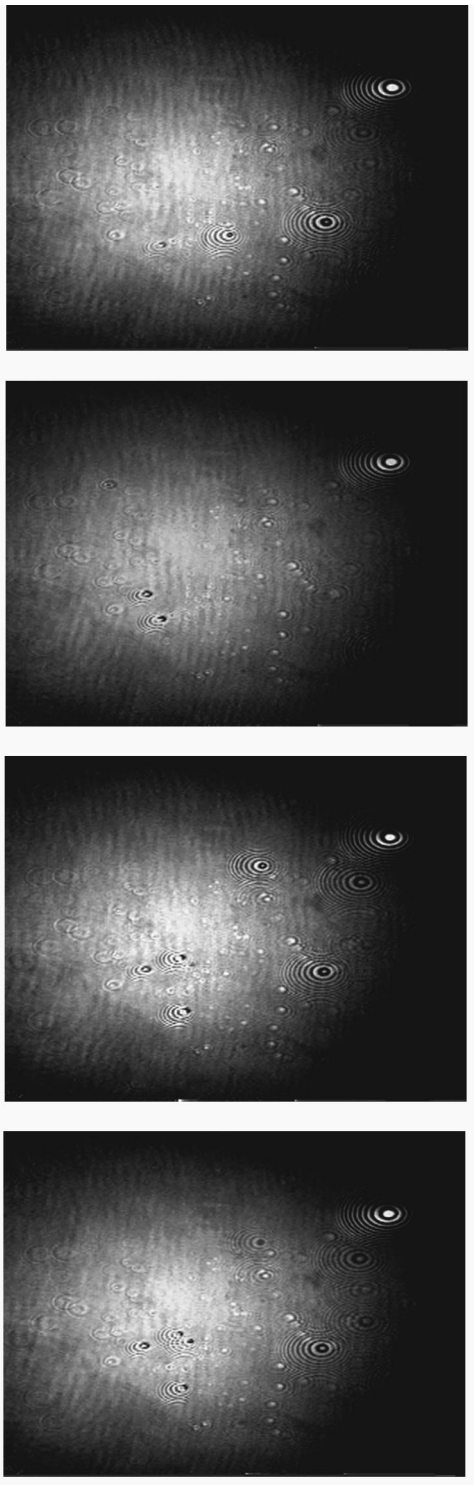

FIG. 12. Four images of a monolayer C_{21} in a period of time less than a second, each one showing different localized oscillations. They can be seen as small holes with newton rings surrounding them. In real time in the BAM, they look like localized blinking Newton rings. Notice that we are looking at the same area of the field of view, as it can be assured by the persistent fixed defects.

a second. Here, some localized oscillations are seen in one of the images, but not in the others. We were unable to measure a characteristic time of oscillation, because the period can go form a half of a second to many oscillation per second, depending on the chosen localized oscillation. The central part of the blinking Newton rings (the holes in the images) has a diameter size of the order of 23–31 μm. Localized oscillations can start at low temperatures ($\sim$2–6 °C), and at low pressures compared with the collapse pressure ($\sim$12 mN/m). However, as the pressure is increased, the number of oscillations sites increases quite notoriously. The oscillations remain for a long time until pressure relaxes. In some cases, these oscillations can be found at the boundary of domains. We made several experiments to find the origin of those oscillations. In some of the experiments, we used subphases previously deaerated to exclude the possibility that bubbles of air formed during the compression, and localized below the monolayer, were the origin of the localized oscillations. Deaeration apparently did not modify the number of localized oscillations when compared with the same experiments, but using nondeaerated subphases. We also prepared the monolayer in different conditions to produce a qualitative modification in the localized oscillation activity. Here, we make a summary of our experiments: (a) A fully expanded monolayer was deposited in a cold subphase (2–6 °C), after a waiting time of the order of 5 h, the compression process started on. In this experiment, the number of localized oscillations decreased notoriously; (b) A fully expanded monolayer was deposited on deaerated warm subphase (45.0 °C), temperature of the subphase was lowered slowly for 2 h. When 2.3 °C was reached, the compression process started on. Here, there was also a notorious reduction of the localized oscillation; (c) A fully expanded monolayer was deposited on a previously deaerated cold subphase (2 to 3 °C), and compressed after the volatile solvent of the spreading solution was evaporated. In this experiment, there were many fixed defects (fixed newton rings), as well as, too many localized oscillations along all the field of view of the BAM; (d) A monolayer was deposited on a cold subphase at (2 to 3 °C), subsequently, the monolayer was compressed up to $\Pi = 25$ mN/m ($\sim$24 Å^2/molec.). The next step in this experiment was to increase temperature slowly up 15.5 °C (2 h), but maintaining fixed the Π. In this experiment, initially, there were too many oscillations, but as temperature was increased the number of localized oscillations decreased, as well as, the area of the monolayer, i.e., there was a loss of molecules in the monolayer. In the same way, as temperature increased, multilayer defects as bright grains and mountain shaped structures increased in number. It is important to mention, that in all experiments if the speed of compression is increased, the same does the number of localized oscillations. These results about the behavior of localized oscillations in C_{21} monolayer suggest that localized oscillations are big areas with a high density of defects (dislocations, disclinations, etc.). Consequently, stress and energy are concentrated in those areas. The monolayer apparently relaxes expelling matter out of the monolayer. Localized oscillations are quite interesting in themselves and they could explain some events previous to the collapse. We are making Langmuir–Blodgett films with monolayers where localized oscillations are found, to study them with atomic force microscopy. This study is underway and will be published shortly.

ACKNOWLEDGMENT

We acknowledge the partial support of DGAPAUNAM project IN103598.

[1] J. Als-Nielsen, D. Jacquemain, K. Kjaer, F. Leveiller, M. Lahav, and L. Leiserowitz, Phys. Rep. **246**, 251 (1994).
[2] C. M. Knobler, in *Advances in Chemical Physic*, edited by I. Prigogine and S. A. Rice (Wiley, New York, 1990), p. 397.
[3] D. Höning and D. Möbius, J. Phys. Chem. **95**, 4590 (1991).
[4] S. Henon and J. Meunier, Rev. Sci. Instrum. **62**, 936 (1991).
[5] E. Stenhagen, in *Determination of Organic Structures by Physical Methods*, edited by E. A. Braude and F. C. Nachord (Academic, New York, 1955).
[6] M. Lundquist, Prog. Chem. Fats other Lipids **16**, 101 (1978).
[7] M. Lundquist, Chem. Scr. **1**, 197 (1971).
[8] A. M. Bibo, C. M. Knobler, and I. R. Peterson, J. Phys. Chem. **95**, 5591 (1991).
[9] D. K. Schwartz, M. W. Tsao, and C. M. Knobler, J. Chem. Phys. **101**, 8258 (1994).
[10] T. M. Fischer, R. F. Bruinsma, and C. M. Knobler, Phys. Rev. E **50**, 413 (1994).
[11] C. M. Knobler, Science **249**, 870 (1990).
[12] D. Andelman, F. Brochard, C. M. Knobler, and F. Rondelez, in *Micelles, Membranes, Microemulsions, and Monolayers*, edited by W. M. Gelbart, A. Ben-Sahul, and D. Roux (Springer, New York, 1994).
[13] M. K. Durbin, A. Malik, A. G. Richter, R. Ghaskadvi, T. Gog, and P. Dutta, J. Chem. Phys. **106**, 8216 (1997).
[14] B. Lin, M. C. Shih, T. M. Bohanon, G. E. Ice, and P. Dutta, Phys. Rev. Lett. **65**, 191 (1990).
[15] D. K. Schwartz and C. M. Knobler, J. Phys. Chem. **97**, 8849 (1993).
[16] M. K. Durbin, A. Malik, R. Ghaskadvi, M. C. Shih, P. Zschack, and P. Dutta, J. Phys. Chem. **98**, 1753 (1994).
[17] G. A. Overbeck and D. Möbius, J. Phys. Chem. **97**, 7999 (1993).
[18] S. Rivière, S. Hénon, J. Meunier, D. K. Schwartz, M. W. Tsao, and C. M. Knobler, J. Chem. Phys. **101**, 10045 (1994).
[19] M. C. Shih, T. M. Bohanon, J. M. Mikrut, P. Zschack, and P. Dutta, Phys. Rev. A **45**, 5734 (1992).
[20] R. M. Kenn, C. Böhm, A. M. Bibo, I. R. Peterson, H. Möhwald, J. Als-Nielsen, and K. Kjaer, J. Phys. Chem. **95**, 2092 (1991).
[21] P. Tippmann-Krayer and H. Möhwald, Langmuir **7**, 2303 (1991).
[22] D. K. Schwartz, M. L. Schlossman, and P. S. Pershan, J. Chem. Phys. **96**, 2356 (1992).
[23] T. M. Bohanon, B. Lin, M. C. Shih, G. E. Ice, and P. Dutta, Phys. Rev. B **41**, 4846 (1990).
[24] M. L. Schlossman, D. K. Schwatz, P. S. Pershan, E. H. Kawanoto, G. J. Kellogg, and S. Lee, Phys. Rev. Lett. **66**, 1599 (1991).
[25] K. Kjaer, J. Als-Nielsen, C. A. Helm, P. Tippmann-Krayer, and H. Möhwald, J. Phys. Chem. **93**, 3200 (1989).
[26] G. A. Overbeck, D. Höning, and D. Möbius, Thin Solid Films **242**, 213 (1994).
[27] S. Rivière-Cantin, S. Hénon, and J. Meunier, Phys. Rev. E **54**, 1683 (1996).
[28] E. Teer, C. M. Knobler, C. Lautz, S. Wurlitzer, J. Kildae, and T. M. Fischer, J. Chem. Phys. **106**, 1913 (1997).
[29] B. Fischer, E. Teer, and C. M. Knobler, J. Chem. Phys. **103**, 2365 (1995).
[30] V. M. Kaganer, I. R. Peterson, R. M. Kenn, M. C. Shih, M. Durbin, and P. Dutta, J. Chem. Phys. **102**, 9412 (1995).